Aspartate Isomerization in the Complementarity-Determining Regions of Two Closely Related Monoclonal Antibodies†

Aditya A. Wakankar,*,‡ Ronald T. Borchardt,§ Charles Eigenbrot,|| Steven Shia,|| Y. John Wang,‡ Steve J. Shire,‡ and Jun L. Liu‡

Late Stage Pharmaceutical and Device Development Group, Genentech Inc., 1 DNA Way, South San Francisco, California 94080, Department of Pharmaceutical Chemistry, The University of Kansas, Lawrence, Kansas 66047, and Department of Protein Engineering, Genentech Inc., 1 DNA Way, South San Francisco, California 94080

Received July 25, 2006; Revised Manuscript Received October 14, 2006

ABSTRACT: The aspartic acid residues (Asp) present in the complementarity-determining regions (CDRs) of the light chains of two recombinant monoclonal antibodies (MAbs), MAb I and MAb II, are highly susceptible to isomerization due to the presence of glycine residues (Gly) on their C-terminal ends. Asp isomerization in these MAbs leads to formation of the isoaspartate (IsoAsp) and the cyclic imide (Asu) variants of these MAbs. Both MAb I and MAb II, employed in this study, elicit their pharmacological responses through binding human IgE. The formation of the MAb variants as a result of Asp isomerization significantly reduces the binding affinities of these antibodies to IgE, thereby reducing their potencies. Here we report on significant differences in the susceptibility of the MAb I and the MAb II to Asp isomerization. The molecular basis for these differences in rates of Asp isomerization was elucidated. The effect of primary sequence on Asp isomerization was evaluated using pentapeptide models of the MAbs, which included the labile Asp residues and their neighboring amino acid residues. The separation of the parent MAbs and pentapeptides from their isomerization products was achieved using hydrophobic interaction chromatography (HIC) and rp-HPLC, respectively. Structural characterization of the MAbs was performed using differential scanning calorimetry (DSC), circular dichroism (CD), and X-ray crystallography. Our investigations demonstrate that the differences in the Asp isomerization rates between MAb I and MAb II can be attributed to structural factors including the conformational flexibility and the extent of solvent exposure of the labile Asp residue.

Recombinant humanized monoclonal antibodies (rhMAbs or MAbs[1]) have evolved into a major class of therapeutics due to their highly selective binding to an antigen, long clearance times, and the possibility of revoking immune cell effector responses (*1*). These therapies include treatment of malignant lymphomas, colorectal carcinomas, allergic asthma, and ulcerative colitis as well as reduction of organ rejection in renal and cardiac transplant patients (*2*−*5*). The MAbs bind the antigen or the ligand through interactions between the residues in the complementarity-determining regions (CDRs) of the antibody and those on the target sites of the antigen. Any modification in the CDR of a MAb due to physical and/or chemical degradation can lead to a loss of the MAb binding affinity for the antigen and, thereby, its potency (*6*, *7*).

MAbs, similar to other proteins, are susceptible to physical degradation processes such as aggregation, denaturation, and precipitation (*8*). The MAbs are also subject to chemical degradation reactions such as deamidation, isomerization, racemization, and oxidation (*6*, *9*, *10*). Nonenzymatic post-translational modification of the Asp residues, resulting in isoaspartate (IsoAsp) and cyclic imide (Asu) products, is a major route of protein degradation both *in vivo* and *in vitro* (*7*, *11*−*13*). Asp isomerization causes problems such as protein aging (*14*). Asp isomerization occurring in protein therapeutics can often lead to a loss of their activities and altered susceptibilities to proteolysis and can potentially trigger autoimmune responses from these therapeutics (*6*, *15*). In the case of MAb I, variants of the MAb that contained isomerization products resulted in an ∼80% loss in the binding affinity of the antibody to IgE (*6*). The variants resulting from the isomerization reaction also present challenges to the manufacturing of antibodies and to the consistency of their formulations (*16*). The impact of Asp isomerization on the safety, efficacy, and shelf life of a protein therapeutic is therefore an important formulation concern.

† This research was a collaborative project between Genentech Inc. and The University of Kansas. This research was conducted in the laboratories of the Late Stage Pharmaceutical and Device Development department at Genentech Inc., 1 DNA Way, South San Francisco, CA 94080.

* Author to whom correspondence should be addressed. E-mail: wakankar.aditya@gene.com. Tel: (650) 225 1000. Fax: (650) 225 7234.

‡ Late Stage Pharmaceutical and Device Development Group, Genentech Inc.

§ The University of Kansas.

|| Department of Protein Engineering, Genentech Inc.

[1] Abbreviations: Asp, aspartate; IsoAsp, isoaspartate; Asu, cyclic imide intermediate; Gly, glycine; CDR, complementarity-determining region; HIC, hydrophobic interaction chromatography; HPLC, high performance liquid chromatography; MAb, monoclonal antibody; CD, circular dichroism; DSC, differential scanning calorimetry.

10.1021/bi061500t CCC: $37.00
Published on Web 01/17/2007

Scheme 1. Pathway for Asp Isomerization in Peptides and MAbs (a) and the Kinetic Model (b) Used in Our Investigations

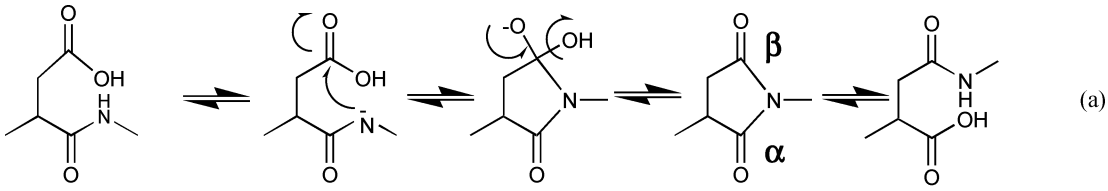

Asp ⇌ Asu ⇌ IsoAsp (b)

$$d(Asp)/dt = -k_{obs}(Asp)$$

The mechanism for Asp isomerization occurring in peptides and proteins was first proposed by Geiger et al. (*17*) and is shown in Scheme 1. Asp isomerization, similar to Asn deamidation, proceeds through a cyclic imide intermediate. This involves nucleophilic attack by the amide backbone nitrogen on the Asp side chain carbonyl to generate the cyclic imide. The cyclic imide then undergoes rapid hydrolytic cleavage at the α or the *β* carbon to form isoaspartate (isoAsp) or aspartate (Asp) products, respectively, in a molar ratio of ∼3:1 at equilibrium. Clarke examined the effect of primary sequence and protein conformation on Asp and Asn degradation in several well-characterized proteins (*13*). These studies suggested two factors to be principal determinants of the susceptibility of an Asp residue to isomerization in proteins: (i) the residue on the C-terminal side of the Asp and (ii) the conformational flexibility of the protein in the region surrounding the Asp (*13*). The effects of C-terminal residues on Asp isomerization have been extensively investigated and well characterized using model hexapeptides (*12*, *18*−*21*). These investigations have shown that the residue on the C-terminal side of the Asp influences Asp isomerization through steric, inductive/electrostatic, and catalytic effects. The studies also indicated that the Asp in an Asp-Gly sequence in proteins was highly susceptible to the isomerization reaction (*12*, *18*−*21*). The effect of local conformation of proteins on Asn deamidation has been widely reported (*22*). Capasso et al. have observed attenuation of deamidation rates in ribonuclease A due to a reduced conformational flexibility of the Asn in proteins compared to peptide models (*23*). Bischoff et al. (*24*) have indicated the importance of local conformational flexibility in a protein as an important determinant of Asn deamidation rate in hirudin. A decrease in Asn deamidation rates due to reduced conformational flexibility in proteins has also been reported for recombinant human lymphotoxin (*25*) and growth hormone releasing factor. Similar to the effects of higher order protein structure on Asn reactivity in proteins, the secondary and the tertiary structure of proteins could also influence the rate of Asp isomerization (*13*). The extensive hydrogen bonding observed in proteins may reduce the flexibility of the Asp residue, leading to an attenuation of isomerization rates in proteins (*13*).

The objective of the current studies was to investigate the rates of Asp isomerization in the two MAbs, MAb I and MAb II, and to elucidate the molecular basis for the rates of Asp isomerization observed in these two MAbs. MAb I and MAb II differ in the primary sequence of their CDR L1 region as shown in Figure 1. The two MAbs also differ in the location of their labile Asp residue with Asp 32 being the labile residue in MAb I and Asp 30 the labile residue in MAb II (Figure 1). The isomerization of Asp 32 in the CDR L1 of MAb I, which led to the formation of IsoAsp and Asu residues, has been reported in samples incubated at pH 5.2 and 37 °C (*6*). Preliminary studies with MAb II under identical pH and temperature conditions have demonstrated that Asp isomerization occurs at Asp 30, leading to the formation of IsoAsp and Asu degradants of MAb II (unpublished work). As mentioned earlier, the Asp isomerization in MAb I (*6*) has been shown to decrease its binding affinity to the human IgE leading to a loss in the potency of this MAb therapeutic.

In this study, the rates of isomerization of the labile Asp residues in MAb I and MAb II were determined as a function of formulation pH. The role of primary sequence, local conformation, and tertiary structure of the MAbs upon Asp isomerization occurring in these biomolecules was assessed. This research advances the understanding of factors governing Asp isomerization in MAbs and provides a basis for protein engineering of MAbs that are less susceptible to Asp isomerization.

EXPERIMENTAL PROCEDURES

Materials. The recombinant humanized monoclonal antibodies MAb I (rhuMAb E25) and MAb II were cloned, expressed, and purified at Genentech (South San Francisco, CA) using identical methodologies. The model peptides VDYDG and VDGEG were synthesized and purified at Genentech. The peptides had their N termini acetylated and their C termini amidated. Papain and anti-papain (Antipain) were purchased from Roche Diagnostics (Mannheim, Germany) and Peptide International (Louisville, KY), respectively. All chemicals and solvents used in making the buffered solutions and mobile phases for chromatography were purchased from Sigma (St. Louis, MO). Water used in these experiments was purified using a Millipore MILLI-Q system.

Formulation Buffers. The formulation buffers were 20 mM acetate (pH 5.0), 20 mM histidine (pH 6.0), and 20 mM phosphate (pH 7.0 and 8.0). The ionic strengths of the

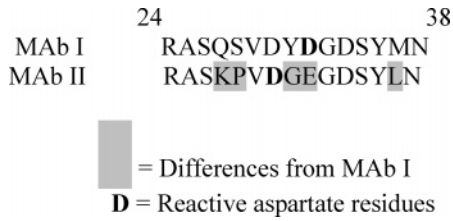

FIGURE 1: The differences between the primary sequences of MAb I and MAb II.

buffered solutions were adjusted to 150 mM with sodium chloride. The concentrations of the buffer components added were corrected for the temperature of the stability studies (50 °C) and the ionic strength (I = 0.15 M) to yield the desired pH. The pHs of the buffers were measured with an Accumet AB15 pH meter.

Stability Studies. MAb solutions ([MAb] = 20 mg/mL) buffered at pH 5, 6, 7, and 8 were prepared for the stability studies. Polypropylene (PP) vials were filled with these solutions and then incubated at 50 °C in a hot air oven. Sample vials were periodically withdrawn and analyzed using HIC assay to monitor the loss of the parent MAbs due to the Asp isomerization. Peptide formulations (0.1 mg/mL) buffered at pH 5, 6, 7, and 8 were placed in PP vials and incubated at 50 °C in the same oven. Sample vials were withdrawn at predetermined time intervals and analyzed using rp-HPLC to monitor loss of the parent peptides due to Asp isomerization. The stability samples were monitored during the initial stages of the degradation reaction and showed ~20−30% loss of the parent forms.

Sample Preparation for HIC (Papain Digestion of MAbs). Papain digest of MAbs was performed prior to HIC. The digestion protocol consisted of incubating the MAbs at 37 °C and pH 7.4 (100 mM Tris) for 2 h in papain (papain: MAb ratio 1:100 w/w), 4 mM EDTA, and 1 mM cysteine. Upon incubation, antipapain (Antipain) was added (papain: antipapain ratio 40:1 w/w) to quench the digestion reaction. The digested samples were then injected onto an HIC column.

HIC of MAbs. The separation and quantitation of the parent MAbs and their IsoAsp and Asu variants were achieved using HIC. Aliquots of the digested MAb (30 μL) were injected onto a TSKGel phenyl-5PW 7.5 × 75 mm column (Fisher Sci., Pittsburgh). Gradient elution was used with solvent A consisting of 2 M ammonium sulfate solution buffered at pH 7.5 and solvent B consisting of 20 mM Tris solution buffered at the same pH. The gradient consisted of varying the concentration of solvent B from 25−100% over a 0 to 50 min time period using a constant flow rate of 1 mL/min. The column was washed for 10 min with 100% solvent B at the end of each run. The column was maintained at 40 °C using a column heater. HIC was performed on a Hewlett-Packard (Palo Alto, CA) 1100 HPLC system, which included a UV detector set at 214 nm for quantitation.

rp-HPLC of Peptides. The parent peptides and their degradation products were separated using an ODS Hypersil C-18, 4.6 × 250 mm column (Fisher Sci., Pittsburgh, PA). The mobile phase consisted of 0.1% v/v trifluoroacetic acid with 8%−15% v/v acetonitrile as the organic phase modifier set at a constant flow rate of 1 mL/min. rp-HPLC was performed using a Hewlett-Packard 1100 HPLC system, which included a UV detector set at 210 nm for quantitation. The degradation products were identified based on the rp-HPLC retention times of the parent and the IsoAsp peptides and the observed product ratios.

Data Analysis. The disappearance of the parent MAbs and the peptides from the solution was fitted to a pseudo-first-order kinetic model. Nonlinear least-squares regression analysis using Origin (Micrococal Software Inc., Northampton, MA) was used to fit the data set and obtain the pseudo-first-order rate constant (k_{obs}). The following equation was used for the fitting:

$$A = A_0 \exp(-k_{obs}t) \quad (1)$$

where A was the concentration of the parent MAb or the peptide at time t, A_0 was the initial concentration of the parent MAb or the peptide.

Protein L-Based Separation of Fab Fragments. The intact MAbs were digested with papain as discussed in the section Sample Preparation for HIC (Papain digestion of MAbs). The Fab fragments were separated using an AffinityPak immobilized protein L column (Pierce Biotechnology, Rockford, IL). The protein L column was washed with binding buffer consisting of 0.1 M phosphate buffer and 0.15 M sodium chloride solution (pH 7.2) prior to loading of the digested MAb onto the column. Upon loading of the digested MAb, the column was further washed with the binding buffer to elute the Fc fragment. The Fab fragment was then eluted from the protein L column using an elution buffer that consisted of 0.1 M glycine solution (pH 2.5). The eluant containing the Fab was then neutralized to pH 7.0 using 1 M Tris buffer and stored at 5 °C prior to crystallization.

X-ray Crystallography of the Fab Fragments. The solutions containing the Fab fragment were dialyzed into 10 mM Hepes, 150 mM sodium chloride (pH 7.2) at 4 °C and then concentrated to 10 mg/mL. Crystals were grown using the sitting drop method by mixing equal quantities of the Fab solution (10 mg/mL) and the ammonium sulfate solution. The crystals obtained were immersed in a cryoprotectant solution containing ammonium sulfate and 20% w/v glycerol and then flash cooled by immersion in liquid nitrogen. Data extending to 2.2 Å (MAb II Fab) and 3.0 Å (MAb I Fab) were collected in space group $P2(1)2(1)2(1)$ at the Advanced Light Source's Berkeley Center for Structural Biology beam line 5.0.1 and reduced using the HKL (*27*) and CCP4 suites (*28*). Structural data was solved by a molecular replacement method that employed the "Phaser" technique (*29*). Structural refinement was performed using CNX (Accelrys, San Diego, CA). Model building and inspection were performed using "XtalView" (*30*).

DSC Analysis. Thermal analysis of MAb I and MAb II was performed using a VP-DSC Micro calorimeter (MicroCal, Northampton, MA). Solutions of the MAbs (1 mg/mL), buffered at pH 5, 6, 7, and 8, were prepared. The solutions were then degassed under vacuum for 15 min at 5 °C. The solutions were scanned in the temperature range 20−100 °C at a scan rate of 50 °C/h. The DSC thermograms were then analyzed using Origin software.

CD Analysis. CD scans of the MAbs were performed in both the far-UV and near-UV regions using a CD spectrophotometer (Aviv, Lakewood, NJ). MAb solutions, buffered at pHs 5, 6, 7 and 8, at concentrations of 1 mg/mL and 20 mg/mL were used to perform CD scans in the far-UV and

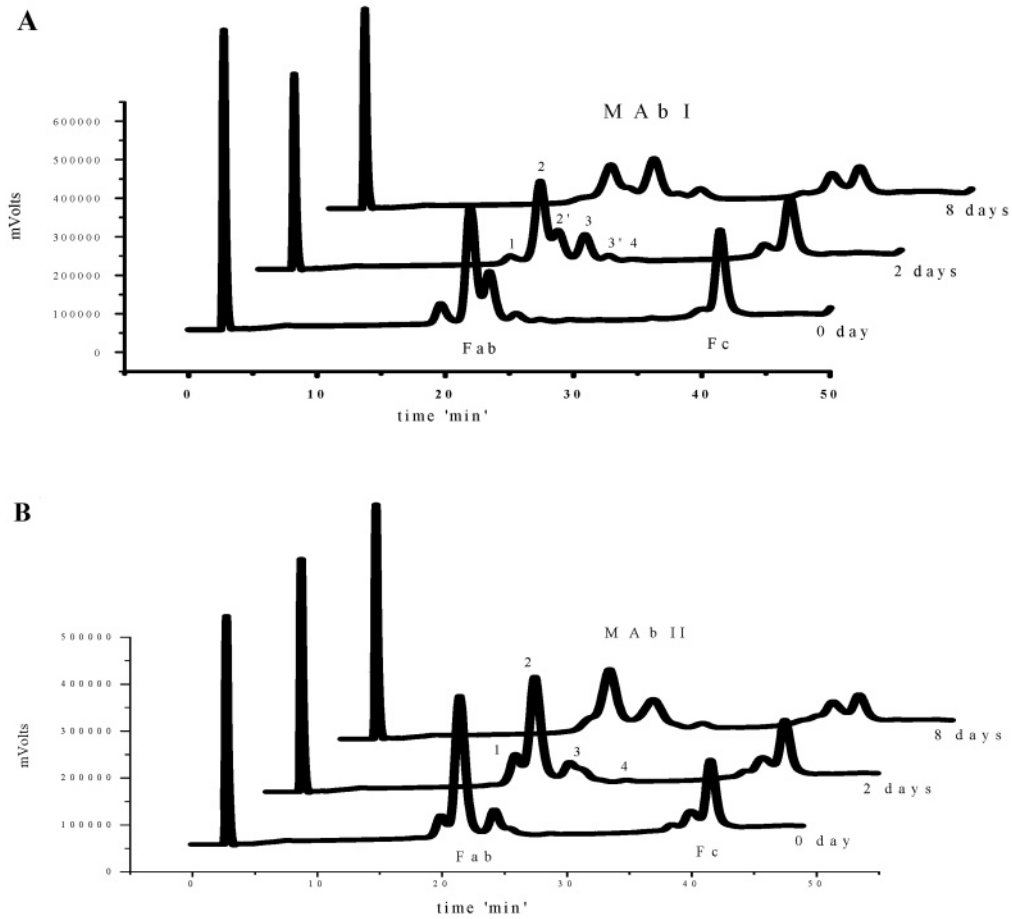

FIGURE 2: HIC elution profiles of MAb I (panel A) and MAb II (panel B) and their variants IsoD32 and AsuD32 in samples incubated in pH 8 buffers at 50 °C for 0, 2, and 8 days. Panel A. Peak 1 was attributed to a nonspecific papain clip in the Fab region of the MAbs; peaks 2 and 2′ were the disulfide and the free thiol forms of the parent MAb I, respectively; peaks 3 and 3′ were the disulfide and the free thiol forms of IsoD32 MAb I, respectively; and peak 4 was the disulfide form of the AsuD32 MAb I. Panel B. The HIC elution profile of MAb II (peak 2) and its variants IsoD30 (peak 3) and AsuD30 (peak 4) in samples incubated in conditions similar to those mentioned for MAb I samples is shown. Peak 1 is the nonspecific papain clip.

near-UV regions, respectively. A scan rate of 0.5 nm/min was employed, and the spectrum for each of the MAbs was corrected for the respective buffer solutions. The bandwidth and the slit size for the instrument were both set at 2 nm. The sample holder was maintained at 25 °C during the scans using a thermostat. Sample cuvettes with 1 mm path length were used. The spectral data obtained were plotted using Origin software.

RESULTS

Analysis of Asp Isomerization in MAbs. The separation and the quantitation of the parent MAbs and their IsoAsp and Asu variants were achieved using an HIC assay (*6*). Figure 2 shows the HIC elution profiles of the Fab and the Fc fragments of MAb I and MAb II sampled at 0, 2, and 8 days of storage at 50 °C and pH 8. These MAb fragments were generated through selective protease digestion of the MAb using papain. Papain cleaves the MAbs on the C-terminal side of His 228 located in the heavy chain region of the MAbs leading to the formation of two Fab fragments and one Fc fragment for each MAb. The MAb digests were then passed through an HIC column, which resulted in the separation of the Fab and Fc fragments. The Fab region of the HIC profile of MAb I showed six distinctive peaks: peak 1 was attributed to a nonspecific papain clip in the Fab region of the MAbs; peaks 2 and 2′ were the disulfide and the free thiol forms of the parent MAb I, respectively; peaks 3 and 3′ were the disulfide and the free thiol forms of IsoAsp MAb I, respectively; and peak 4 was the disulfide form of the Asu MAb I. The free thiol form of Asu MAb I was not detectable. The disulfide forms of the MAbs arise from an intrachain disulfide bond between residues Cys 22 and Cys 26 in the heavy chain region of the Fabs, and the free thiol forms were the MAbs with the disulfide bond reduced. The identities of the individual peaks in the HIC profile were established from earlier work that involved tryptic mapping, mass spectrometry, and N-terminal sequencing of the different peaks in the HIC profile (*6*). The Asp isomerization rates of the disulfide and the free thiol form of the MAbs were compared and observed to be identical (data not shown). For the purpose of our studies, the free thiol and the disulfide forms of the parent MAbs were considered to be kinetically equivalent.

To investigate the Asp isomerization in MAb I, the changes in the Fab region of the HIC profile were monitored. The loss of Asp 32 in MAb I (peaks 2 and 2′) and the formation of IsoAsp 32 (peaks 3 and 3′) and Asu 32 (peak 4) variants were monitored as a function of time. The changes in the peak areas of MAb I and its degradants, which were observed as a function of incubation time, demonstrate the

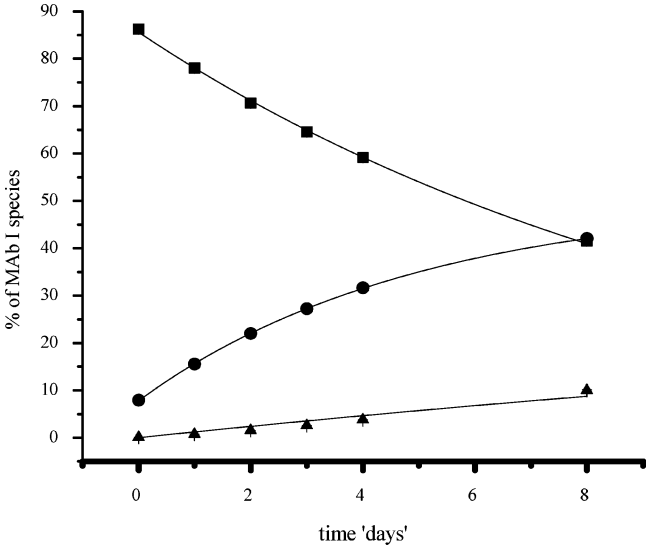

FIGURE 3: A time course for the disappearance of the parent MAb I (■) and the appearance of its IsoD32 (●) and AsuD32 (▲) degradation products in samples incubated in pH 8 buffers at 50 °C.

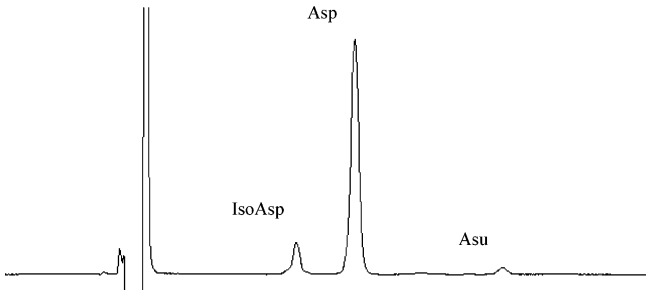

FIGURE 4: rp-HPLC elution profile of VDYDG and its degradation products VDYIsoDG and VDYAsuDG in samples incubated for 2 days in pH 8 buffers at 50 °C.

utility of HIC for monitoring this isomerization reaction (Figure 2). As shown in Figure 2, the HIC elution profile for MAb II was similar to that observed for MAb I except for the absence of the free thiol form in the Asp and the IsoAsp species of MAb II. The identity of individual peaks in the MAb II elution profile was based on results from tryptic mapping, mass spectrometry, and protein sequencing studies (unpublished data).

Figure 3 shows the time course for the disappearance of Asp 32 in MAb I and the appearance of its IsoAsp 32 and Asu 32 degradation products. As shown in the figure, an increase in the concentration of Asu 32 product was observed with time. However, this increase in Asu product is modest at pH 8 relative to the increase observed at lower pHs. This is expected since the Asu product is unstable at higher pHs and therefore undergoes rapid hydrolysis under these conditions. The loss of parent MAb I was fitted to a pseudo-first-order rate model to obtain the apparent isomerization rate constant (k_{obs}). The k_{obs} values were obtained for both MAbs at different pH values and were plotted as a function of pH (Figure 6).

Analysis of Asp Isomerization in Peptides. For the purpose of evaluating the role of primary sequence on Asp isomerization, we synthesized pentapeptides VDYDG and VDGEG, which consisted of residues 29 to 33 in MAb I and Mab II, respectively. These peptide models permitted determination

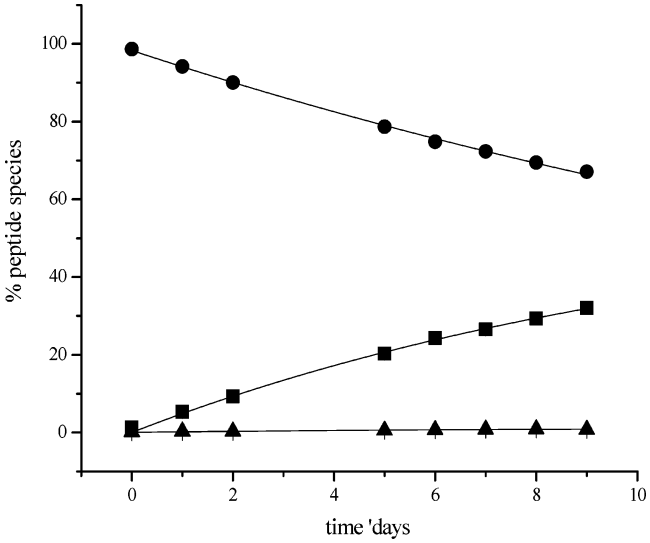

FIGURE 5: A time course for the disappearance of the parent peptide VDYDG (●) and the appearance of its degradation products VDYIsoDG (■) and VDYAsuDG (▲) in samples incubated in pH 8 buffers at 50 °C.

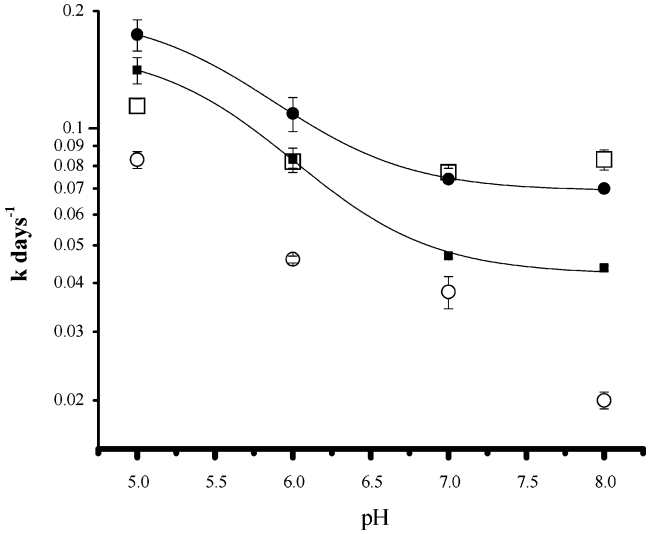

FIGURE 6: The pH−rate profiles for Asp isomerization occurring in MAb I (□) and MAb II (○) and the peptide models VDYDG (■), for MAb I, and VDGEG (●), for MAb II, are shown. The k_{obs} values for plotting the pH−rate profiles were obtained by pseudo-first-order fits to the data obtained from the stability studies conducted with the MAb and peptide samples. The solid lines were fitted to the data by nonlinear regression analysis using the equation $k_{obs} = (K_a/[H^+] + K_a)(k_H{}^+[H^+] + k_o)$ where K_a is kinetic dissociation rate constant, $k_H{}^+$ is the rate constant for acid catalyzed attack on the ionized aspartate, and k_o is a rate constant that includes contributions from both acid and base catalyzed attack on the ionized aspartate. The stability studies were performed by buffering the MAb and peptide samples in pH 5, 6, 7 and 8 buffers ([buffer] = 20 mM, I = 150 mM) and then incubating the samples at 50 °C.

of the role of the residues neighboring to the labile Asp residues on their isomerization rates without the complications associated with the structural features of the MAbs. Both peptides had their N and C termini blocked to eliminate possible effects of terminal charges on the Asp isomerization rates.

An rp-HPLC method was developed for separation of the parent peptides and their degradation products. The degradation products were identified based on the rp-HPLC elution

profiles of VDYIsoDG and VIsoDGEG, the product ratios, and the rp-HPLC elution profiles reported for Asp-containing peptides undergoing isomerization (*20*). The rp-HPLC elution profile of VDYDG upon incubation at 50 °C and pH 8 for 2 days is shown in Figure 4. The elution profiles for VDGEG and its degradation products were similar to those of VDYDG and its degradants (data not shown). The IsoAsp degradants were the predominant products arising from these peptide models at all pHs studied except pH 5, where significant amounts of the Asu degradants were also detected. The loss of the parent peptide, as shown in Figure 5, was fitted to a pseudo-first-order rate equation (eq 1), and the k_{obs} values were calculated. The k_{obs} values obtained at different pHs were then used to generate the pH−rate profiles for the two peptides (Figure 6).

pH−Rate Profile of Asp Isomerization in Peptide Models

The pH−rate profiles obtained for the peptides VDYDG and VDGEG are shown in Figure 6. Both the pH−rate profiles show a pH-dependent region in the pH range of 5 to 7. Further increases in pH result in the isomerization rates becoming pH-independent. Oliyai et al. (*20*) have studied the pH dependency of Asp isomerization in the peptide VYPDGA. Our results for the pH dependency of isomerization rates in VDYDG and VDGEG are in agreement with their observations. A comparison of the pH−rate profiles of VDYDG and VDGEG also revealed that the isomerization rates of VDGEG were faster than the isomerization rates of VDYDG at all pHs investigated.

pH−Rate Profile of Asp Isomerization in MAbs

The pH−rate profiles of Asp isomerization in the MAbs are illustrated in Figure 6. A comparison of the profiles for the two MAbs indicate the following: (i) the isomerization rates of MAb I were faster than those observed for MAb II at all pHs investigated; (ii) the isomerization rates of MAb I were less affected by changes in pH than were those of MAb II; and (iii) MAb II showed increased stability to isomerization at higher pH.

A comparison of isomerization rates between MAb I and its peptide model VDYDG showed that Asp isomerization in the antibody was faster than that of the peptide at pH > 6. A similar comparison between the isomerization rates of MAb II and its peptide model VDGEG showed Asp isomerization rates in the antibody to be slower than those of the peptide at all pHs investigated.

Biophysical Characterization of MAbs

DSC Analysis. DSC of the MAbs was performed to examine the potential role of the structural stability of the antibodies in their susceptibilities to chemical degradation, i.e., Asp isomerization. The DSC thermograms were obtained in the pH range of 5 to 8. The DSC thermograms for the antibodies at pH 5 and 8 are as shown in Figures 7 and 8, respectively. At pH 5, the DSC thermograms of both MAbs showed four transitions: (i) an Fc melting transition at 65 °C; (ii) a second Fc melting transition at 77 °C; and (iii) a Fab melting transition at 83 °C that coincided with transition (iv), which was an exothermic transition due to MAb aggregation (unpublished data wherein assignments of Fab and Fc transitions were determined using isolated Fab and Fc samples of several MAbs). The thermograms for the two MAbs at pH 6 were identical to those observed at pH 5. At pH 8, the DSC thermograms showed two transitions for MAb I and three transitions for MAb II. The DSC thermograms for MAb I showed an Fc melting transition and a Fab melting transition. The DSC thermograms for MAb II also showed an Fc and a Fab transition in addition to an exothermic transition due to MAb aggregation. The low-temperature Fc transition at 65 °C was not observed in either MAb. The melting temperature of the Fab transition for MAb I decreased by 5 °C following an increase in pH from 5 to 8. The temperature of the Fab transition for MAb II was unaffected by a similar change in pH. The DSC curves obtained at pH 7 for the two MAbs were similar to those reported at pH 8 (data not shown).

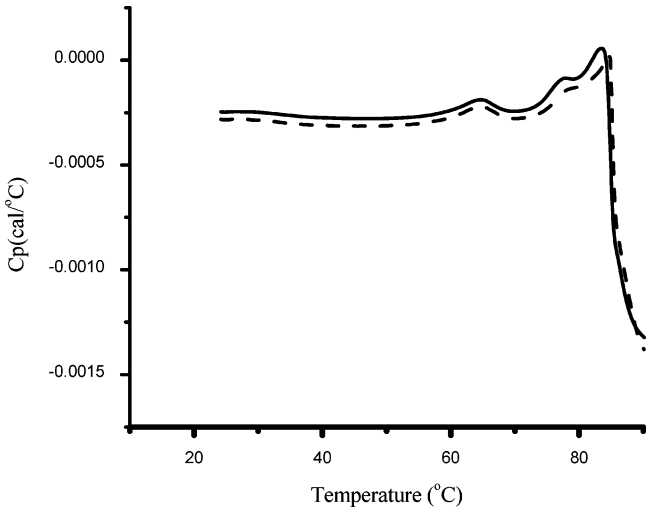

FIGURE 7: The DSC melting curves of MAb I (solid line) and MAb II (dashed line) in solutions buffered at pH 5 ([buffer] = 20 mM, I = 150 mM).

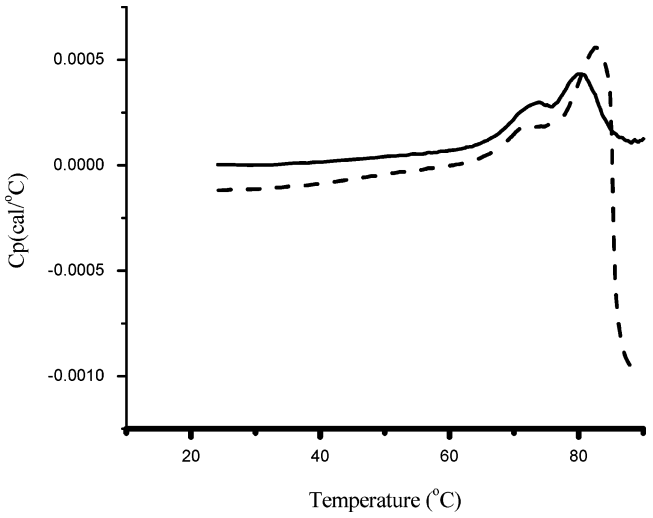

FIGURE 8: The DSC melting curves of MAb I (solid line) and MAb II (dashed line) in solutions buffered at pH 8 ([buffer] = 20 mM, I = 150 mM).

CD Analysis. The secondary and the tertiary structure of the MAbs were evaluated using far-UV and near-UV CD, respectively. The CD spectra for MAb I and MAb II, in both the far-UV and near-UV regions, were identical at pH 8 as well as at other pHs under investigation (data not shown). The CD analysis was not suggestive of any significant

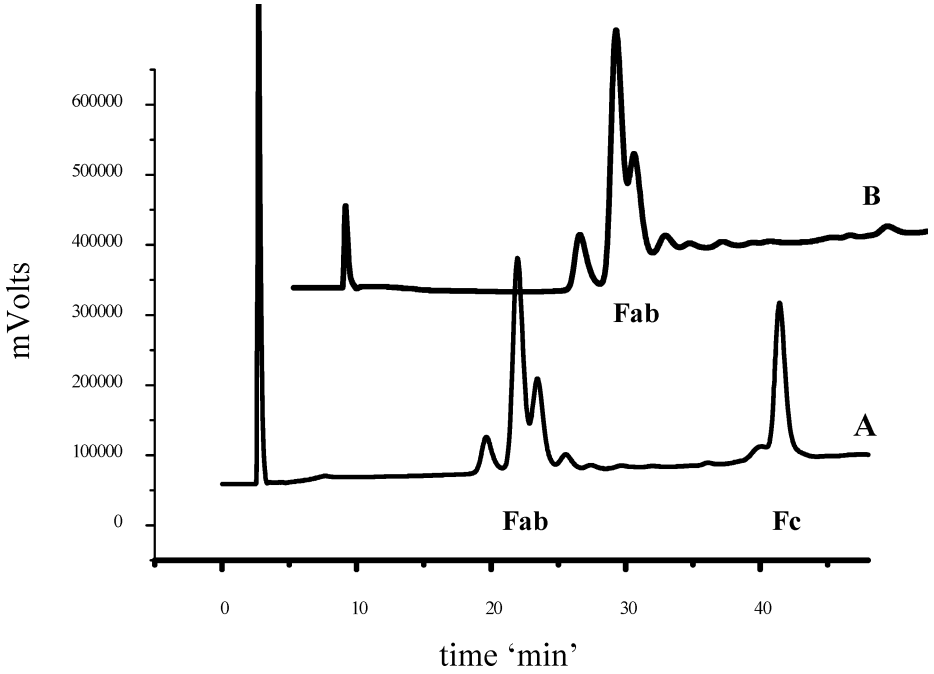

FIGURE 9: The HIC elution profiles of MAb I following papain digestion of the MAb (A), and after separation of the papain digest using a protein L column (B).

differences in the secondary and the tertiary structures of the two Mabs (data not shown).

Determination of Local MAb Structure Using X-ray Crystallography

Separation of Fab Portions of MAbs Using a Protein L Column. The intact MAbs were digested with papain. The Fab portions were then separated from the Fc portions using a protein L column. Protein L specifically binds to the Fab in the kappa light chain region and thus provides an efficient method for separation of the Fab and the Fc regions in MAb following papain digestion. As shown in Figure 9, the separation of the Fab fragment was confirmed by injection of the papain-digested MAb and the purified Fab fragment onto an HIC column.

X-ray Crystallographic Structures of MAb I and MAb II. X-ray crystal structures of the Fab regions of the MAbs were determined since the Fabs were easier to crystallize than were the MAbs. Prior to crystallization, the Fab fragment was purified from the Fc fragment using protein L chromatography post papain digestion of the MAbs. As shown in Figure 9, successful purification of the Fab portions of both the MAbs was achieved using this technique.

Upon purification, the Fabs were crystallized and X-ray crystal structures were obtained. X-ray crystal structure data extending to resolutions of 3.0 Å and 2.2 Å were obtained for the Fabs of MAb I and MAb II, respectively (Figures 10a and 10b). The solvent accessibility parameters were determined for residues 29 to 33 for each of the MAbs (Table 1) (*31*). Based on these solvent accessibility parameter values (Table 1), the labile Asp in MAb I (Asp 32) was observed to be located in a more solvent-exposed region of the antibody whereas the labile Asp in MAb II (Asp 30) was considerably more buried.

To examine the possible influence of MAb conformation on the Asp isomerization rates in MAbs, we compared the local structures consisting of the CDR residues 29 to 33 of the two MAbs (Figures 10a and 10b). The structure shows residues 29 to 32 in a type I β turn in both MAbs. The structure also revealed that the labile Asp (Asp 32) in MAb I was more exposed to a solvent environment than the labile Asp (Asp 30) in MAb II. The distances between the Asp side chain carbonyl and the succeeding amide nitrogen atom were measured using the crystal structure data. These distances were 5.1 Å in MAb I and 5.4 Å in MAb II. Proximity between the side chain carbonyl and the amide nitrogen would ease the formation of the cyclic imide and lead to faster Asp reactivity (*13*). The fact that these distances are comparable would suggest similar reactivity for the two Asp residues and thus does not explain the observed trend in isomerization rates for these MAbs.

From the X-ray crystal structure data, the atomic displacement parameters, the *B* values, were determined for each atom in the amino acid sequence 29 to 33 for both MAbs. The *B* values of the β carbons of residues 30 and 32 of the MAbs were used as indicators of the conformational flexibility of their side chains (Table 2). The *B* values obtained from the X-ray crystal structure of MAb I could not be used to indicate local flexibilities due to the lower structural resolution obtained for this structure. The variability in the *B* values associated with the MAb I structure far exceeded the differences in *B* values observed between the β carbon atoms of residues at positions 30 and 32. A higher structural resolution of the MAb II X-ray crystal structure resulted in lower variability for the *B* values obtained for MAb II. The *B* values obtained from the MAb II X-ray crystal structure could then be used for estimating local flexibilities along a MAb sequence. The *B* value for the β carbon of the residue at position 30 was considerably lower than the *B* value for the β carbon of the residue at position 32 in MAb II. This observation suggests lower conformational flexibility of the side chain of the residue at position 30 compared to that of the residue at position 32 in MAb II.

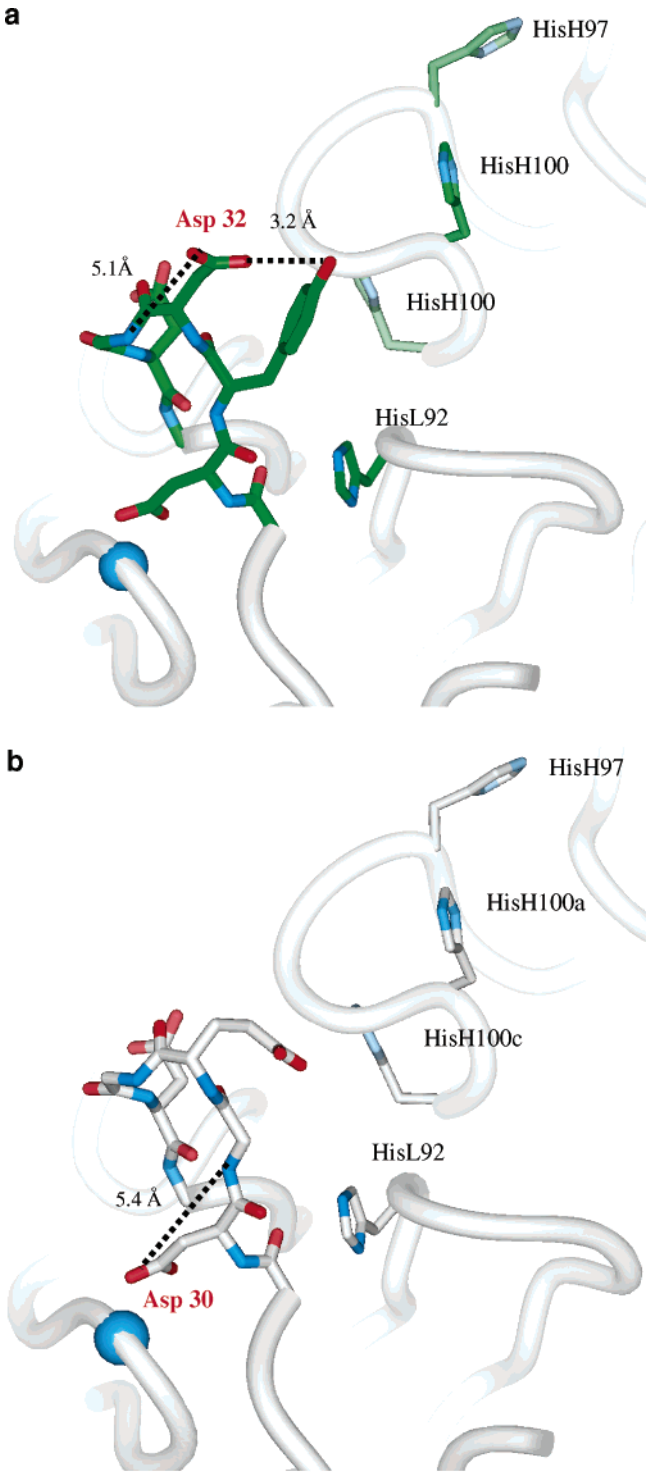

FIGURE 10: (a) X-ray crystal structure of the CDR L1 region (residues 29 to 33) of MAb I. (b) X-ray crystal structure of the CDR L1 region (residues 29 to 33) of MAb II.

DISCUSSION

Asp isomerization in the CDR L1 regions of MAb I and MAb II leads to the formation of IsoAsp and Asu variants, causes a loss of binding affinity of these antibodies to human IgE (*6*, unpublished work). The MAbs differ in primary sequence of their CDR L1 regions and the location of the labile Asp residues as shown in Figure 1. Asp 32 is the labile residue in MAb I, and Asp 30 is the labile residue in MAb II. These two labile Asp residues are followed by Gly residues on their C-terminal side. This primary sequence information would suggest that the rate of Asp isomerization in MAb I would not be significantly different from the rate of Asp isomerization in MAb II. However, our data show that the isomerization rate in MAb I is faster than the isomerization rate in MAb II. This observation suggests that the primary sequence effects may not be the only factors governing isomerization rates in these MAbs. Local conformational differences in these MAbs could be another important factor determining the rates of isomerization in these biomolecules.

Table 1: Solvent Accessibility Parameters[a] of the Amino Acid Residues 29 to 33 of MAb I and MAb II

MAb I		MAb II	
residue	solvent accessibility parameter (%)	residue	solvent accessibility parameter (%)
Val 29	0	Val 29	0
Asp 30	37.2	Asp 30	39.1
Tyr 31	54.5	Gly 31	10.2
Asp 32	71.3	Glu 32	77.9
Gly 33	94.4	Gly 33	95.9

[a] Reference *31*.

Table 2: *B* Values[a] of the β Carbons of the Asp and the Glu Residues

MAb I		MAb II	
residue	*B* values	residue	*B* values
Asp 30	32.7 ± 16	Asp 30	50.3 ± 6
Asp 32	49.8 ± 16	Glu 32	66.4 ± 6

[a] The *B* values for the β carbons of the Asp and the Glu residues were determined on the basis of the X-ray crystal structures of MAb I and MAb II.

Peptide models VDYDG and VDGEG, encompassing residues 29 to 33 in the CDR L1 region of MAb I and MAb II, respectively, were synthesized and their kinetics of Asp isomerization determined. Peptide models have been shown to be useful tools in developing a mechanistic understanding of reactions such as deamidation of Asn residues and isomerization of Asp residues (*12*, *17*, *20*). The use of peptide models precludes the potential effects of higher order structure of proteins on Asp isomerization rates and enables determination of the effects of primary sequence on the isomerization reaction (*12*). The disappearance of the parent peptides and the appearance of the degradants were monitored using an rp-HPLC assay. The rp-HPLC profile shown in Figure 4 illustrates the separation of the parent peptides from their IsoAsp and Asu products. Based on a comparison of the degradation profiles for the MAbs and their peptide models, the distribution of the IsoAsp products and the Asu products formed during Asp isomerization was similar in both the MAbs and the peptides (Figures 3 and 5). This demonstrates that the mechanism for Asp isomerization in peptide models is similar to mechanism of Asp isomerization in the Mabs.

In previous literature reports, the rates of Asp isomerization in peptides have been determined using pseudo-first-order reversible reaction rate models (*17*, *20*). These reports along with other published literature on peptide and protein deamidation/isomerization have demonstrated that contributions of the forward reaction, the formation of the IsoAsp from the Asp, to the observed isomerization rate are ~3- to

4-fold greater those of the reverse reaction, the formation of the Asp from the IsoAsp (*17*, *20*, *32*). One limitation in the present study was that isomerization in the antibodies could not be monitored till equilibrium concentrations of the Asp and the IsoAsp species were attained. A significant degree of protein precipitation (>20%) was detected in antibody samples maintained at 50 °C for a period beyond 12 days (data not shown). Thus, the isomerization reaction was monitored in both peptides and proteins during the initial stages of reaction (~30% isomerization). The isomerization data obtained from these stability studies were fitted to a pseudo-first-order kinetic model based on the assumption that the contributions of the reverse reaction to the observed isomerization rate (k_{obs}) are minimal during the initial stages of the reaction. The rates of Asp isomerization (k_{obs}) obtained from pseudo-first-order fits to the peptide and MAb stability data were used for comparing Asp reactivity among these biomolecules.

The rates of Asp isomerization (k_{obs}) obtained from pseudo-first-order fits to the peptide and MAb stability data at pH 5, 6, 7, and 8 were used to generate the pH−rate profiles shown in Figure 6. The pH−rate profiles for the peptide models were similar to the pH−rate profiles reported earlier for the peptide VYPDGA in the pH range of 5 to 8 (*20*). The residue on the C-terminal side of an Asp has a major influence on its isomerization kinetics, and the residue on the N-terminal end has a minor influence on Asp isomerization (*12*). The labile Asp residues in both the peptides are followed by a Gly residue on their C-terminal side. The similarity in the C-terminal residue would suggest similar chemical reactivities of the Asp residues in the two MAb peptide models. However, a small difference in the isomerization rates was observed between the two MAbs peptide models; specifically, the rate of Asp isomerization in VDYDG was slower than the rate of Asp isomerization in VDGEG. This difference in isomerization rates could be due to a difference in the residues N-terminal to the labile Asp residues for the two peptides. The residue N-terminal to the labile Asp in VDYDG, which is Tyr, could sterically hinder the reactivity of Asp, which leads to a decrease in isomerization rates (*12*).

As shown in Figure 6, the isomerization rates of MAb I were faster than those of MAb II throughout the pH range studied. This was the opposite of what was observed for the peptide models, where the isomerization rates in the peptide model for MAb I were slower than the isomerization rates in the peptide model for MAb II. The fact that the trend in isomerization rates for MAbs does not correlate with the trend observed for their respective peptide models suggests that the primary sequence of the MAbs is not the only factor that determines the isomerization rates in these biomolecules.

The isomerization rates in MAb I were less pH-dependent than in its peptide model. As shown in Figure 6, at pH > 6, the isomerization rates in MAb I were faster than those observed for its peptide model. Previous studies have shown that the rates of deamidation and isomerization are significantly slower in proteins compared to their peptide models due to structural effects (*13*, *23*, *25*, *26*). Structural stability and conformational effects in proteins are known to be responsible for this attenuation in the isomerization rates (*23*, *33*). The fact that the isomerization rates in MAb I are faster than those in its peptide model could suggest a potential catalytic effect due to secondary or tertiary structural features found in the protein. The Asp isomerization rates for MAb II and its peptide model showed an attenuation in isomerization rates as pH was increased. As was expected, the isomerization rates in MAb II were slower than those in its peptide model.

To evaluate the potential effects of MAb secondary and tertiary structure and its conformational stability on Asp isomerization rates, CD and DSC analyses of the two MAbs at pHs 5, 6, 7, and 8 were performed. The DSC thermograms (Figure 7) obtained for the two MAbs at pH 5 demonstrate comparable structural stability of the two MAbs since the Fc and the Fab melting transitions for the MAbs occur at the same temperatures. A comparison of the DSC thermograms at pH 5 and 8 for MAb I (Figure 8) indicates decreased structural stability of the MAb I Fab at pH 8 compared to its structural stability at pH 5. This decreased structural stability at higher pHs in MAb I Fab also correlated with its increased susceptibility to Asp isomerization at higher pH.

A comparison of the CD spectra of the two MAbs, in both the far UV and the near UV regions, demonstrates similarity in the secondary and the tertiary structure of Mabs (data not shown). The CD spectra observed for both the MAbs in the far UV region show predominantly a β-sheet structure that is consistent with other MAbs of its class (*34*). The CD spectra determined at pH 8 for the two MAbs were consistent with those observed in the pH range 5 to 7 (data not shown). These observations suggest that the pH of the formulation does not alter the secondary or the tertiary structural characteristics of the MAbs.

The possible influence of the local conformation around the labile Asp residues in these MAbs was investigated using X-ray crystal structures. Based on the X-ray crystal structure, the solvent accessibilities of residues 29 to 33 were calculated using the method developed by Lee and Richards (*31*). The results from these calculations are summarized in Table 1. The solvent accessibilities of the residues increased with increasing residue number from 29 to 33 in both MAbs. The results demonstrate that the Asp residue in MAb I (residue 32) lies in the more solvent-exposed regions of the β turn compared to the Asp in MAb II (residue 30). The regions with greater solvent accessibility are also likely to be associated with more flexible regions in a protein (*35*).

The local flexibilities of the amino acid residues were determined using the *B* values. The *B* values of the β carbons of residues at position 30 and 32 were used as indicators of the flexibilities of their respective side chains. The goal was to compare local flexibility of residue 32 in MAb I to that of residue 30 of MAb II. However, due to differences associated with X-ray crystal structure resolution of MAb I and MAb II this goal was altered to comparing local flexibility of residue 30 to that of residue 32 within each Fab structure. The *B* values of the β carbons of residue 30 and residue 32 in MAb I and MAb II are shown in Table 2. The *B* values of the β carbons in MAb II demonstrate that residue 30 lies in less flexible regions of the MAb than does residue 32. The lesser local flexibility at residue 30 in MAb II (Table 2) also correlates with its lower solvent accessibility (Table 1). The local flexibilities of residues 30 and 32 in MAb I could not be accurately determined due to lower resolution of the MAb I X-ray structure. The lower resolution in the X-ray crystal structure of the MAb I led to increased

variability in the *B* values. The variability in the *B* values for the MAb I X-ray crystal structure far exceeded the differences in the *B* values observed for the β carbon atoms of residues 30 and 32 (Table 2). Therefore, for MAb I structure we assumed that residue 32 would be more flexible than residue 30 based on its higher solvent accessibility. This assumption is based on correlations observed between solvent accessibility and residue flexibility for the MAb II structure and similar correlations reported for other protein structures (*35*). In the case of MAb I, the greater flexibility of Asp residue 32 will decrease the energy required for its cyclization to Asu in the MAb. As shown in Scheme 1, the rate-determining step in the isomerization pathway was the cyclization step and, thus, greater flexibility of the Asp would lead to faster reactivity to isomerization. This was in agreement with the results from our kinetic studies (Figure 6).

Based on the pH−rate profile (Figure 6), the Asp isomerization rates in MAb I were faster than those in its peptide model VDYDG under neutral-to-basic conditions (pHs > 6). Residues that H-bond to a labile Asp in proteins could catalyze its reactivity to isomerization (*36*). The X-ray crystal structure for MAb I shows a Tyr residue located within H-bonding distance of the labile Asp residue (Figure 10a). The presence of an H-bond-donating residue such as Tyr could potentially catalyze Asp reactivity, especially under pH conditions where the Asp is ionized, i.e., at pH > pKa of the Asp (pH > 4). The lack of a similar catalytic effect in peptide model VDYDG could be attributed to the flexibility of the peptide which does not favor a stable H-bond formation between the Asp and the Tyr.

This research demonstrates that the reactivity of the Asp residues to isomerization in MAbs not only is affected by their primary sequences but also is a function of the solvent accessibility (as per X-ray crystallography) and the local conformational flexibility (as per *B* values) of the Asp residues. Greater solvent accessibility and therefore greater flexibility of the Asp lead to an increase in its reactivity. A decrease in the MAb structural stability (as per DSC) and the presence of H-bond-donating residues within close proximity to a labile Asp (as per X-ray crystal structure) could accelerate Asp reactivity in MAbs.

ACKNOWLEDGMENT

The authors thank Mary Nguyen and Brian Lobo of the Late Stage Pharmaceutical and Device Development Department and Reed Harris, Armando Cordoba, and Rodney Keck of the Analytical Chemistry Department at Genentech Inc. for their assistance with the various experimental techniques. The authors also express thanks to Clifford Quan from the Medicinal Chemistry Department at Genentech Inc. for synthesizing the peptide models.

REFERENCES

1. Ludwig, D. L., Pereira, D. S., Zhu, Z., Hicklin, D. J., and Bohlen, P. (2003) Monoclonal antibody therapeutics and apoptosis, *Oncogene 22*, 9097−9106.
2. Chong, G., Lee, F. T., Hopkins, W., Tebbutt, N., Cebon, J. S., Mountain, A. J., Chappell, B., Papenfuss, A., Schleyer, P., U, P., Murphy, R., Wirth, V., Smyth, F. E., Potasz, N., Poon, A., Davis, I. D., Saunder, T., O'Keefe, G, J., Burgess, A. W., Hoffman, E. W., Old, L. J., and Scott, A. M. (2005) Phase I trial of 131I-huA33 in patients with advanced colorectal carcinoma, *Clin. Cancer Res. 11*, 4818−4826.
3. Feagan, B. G., Greenberg, G. R., Wild, G., Fedorak, R. N., Pare, P., McDonald, J. W., Dube, R., Cohen, A., Steinhart, A. H., Landau, S., Aguzzi, R. A., Fox, I. H., and Vandervoort, M. K. (2005) Treatment of ulcerative colitis with a humanized antibody to the alpha4beta7 integrin, *N. Engl. J. Med. 352*, 2499−2507.
4. Hershberger, R. E., Starling, R. C., Eisen, H. J., Bergh, C. H., Kormos, R. L., Love, R. B., Van Bakel, A., Gordon, R. D., Popat, R., Cockey, L., and Mamelok, R. D. (2005) Daclizumab to prevent rejection after cardiac transplantation, *N. Engl. J. Med. 352*, 2705−2713.
5. Holgate, S. T., Djukanovic, R., Casale, T., and Bousquet, J. (2005) Anti-immunoglobulin E treatment with omalizumab in allergic diseases: an update on anti-inflammatory activity and clinical efficacy, *Clin. Exp. Allergy 35*, 408−416.
6. Cacia, J., Keck, R., Presta, L. G., and Frenz, J. (1996) Isomerization of an aspartic acid residue in the complementarity-determining regions of a recombinant antibody to human IgE: identification and effect on binding affinity, *Biochemistry 35*, 1897−1903.
7. Huang, L., Lu, J., Wroblewski, V. J., Beals, J. M., and Riggin, R. M. (2005) In vivo deamidation characterization of monoclonal antibody by LC/MS/MS, *Anal. Chem. 77*, 1432−1439.
8. Mahler, H.-C., Mueller, R., Friess, W., Delille, A., and Matheus, S. (2005) Induction and analysis of aggregates in a liquid IgG1-antibody formulation, *Eur. J. Pharm. Biopharm. 59*, 407−417.
9. Chelius, D., Rehder, D. S., and Bondarenko, P. V. (2005) Identification and Characterization of Deamidation Sites in the Conserved Regions of Human Immunoglobulin Gamma Antibodies, *Anal. Chem. 77*, 6004−6011.
10. Lam, X. M., Yang, J. Y., and Cleland, J. L. (1997) Antioxidants for prevention of methionine oxidation in recombinant monoclonal antibody HER2, *J. Pharm. Sci. 86*, 1250−1255.
11. Zhang, W., Czupryn, J. M., Boyle, P. T., Jr., and Amari, J. (2002)-Characterization of asparagine deamidation and aspartate isomerization in recombinant human interleukin-11, *Pharm. Res. 19*, 1223−1231.
12. Robinson, N. E., and Robinson, A. B. (2001) Molecular clocks, *Proc. Natl. Acad. Sci. U.S.A. 98*, 944−949.
13. Clarke, S. (1987) Propensity for spontaneous succinimide formation from aspartyl and asparaginyl residues in cellular proteins, *Int. J. Pept. Protein Res. 30*, 808−821.
14. Reissner, K. J., and Aswad, D. W. (2003) Deamidation and isoaspartate formation in proteins: unwanted alterations or surreptitious signals?, *Cell. Mol. Life Sci. 60*, 1281−1295.
15. Aswad, D. W., Paranandi, M. V., and Schurter, B. T. (2000) Isoaspartate in peptides and proteins: formation, significance, and analysis, *J. Pharm. Biomed. Anal. 21*, 1129−1136.
16. Harris, R. J., Kabakoff, B., Macchi, F. D., Shen, F. J., Kwong, M., Andya, J. D., Shire, S. J., Bjork, N., Totpal, K., and Chen, A. B. (2001) Identification of multiple sources of charge heterogeneity in a recombinant antibody, *J. Chromatogr. B Biomed. Sci. Appl. 752*, 233−245.
17. Geiger, T., and Clarke, S. (1987) Deamidation, isomerization, and racemization at asparaginyl and aspartyl residues in peptides. Succinimide-linked reactions that contribute to protein degradation, *J. Biol. Chem. 262*, 785−794.
18. Stephenson, R. C., and Clarke, S. (1989) Succinimide formation from aspartyl and asparaginyl peptides as a model for the spontaneous degradation of proteins, *J. Biol. Chem. 264*, 6164−6170.
19. Radkiewicz, J. L., Zipse, H., Clarke, S., and Houk, K. N. (2001) Neighboring side chain effects on asparaginyl and aspartyl degradation: an ab initio study of the relationship between peptide conformation and backbone NH acidity, *J. Am. Chem. Soc. 123*, 3499−3506.
20. Oliyai, C., and Borchardt, R. T. (1993) Chemical pathways of peptide degradation. IV. Pathways, kinetics, and mechanism of degradation of an aspartyl residue in a model hexapeptide, *Pharm. Res. 10*, 95−102.
21. Oliyai, C., and Borchardt, R. T. (1994) Chemical pathways of peptide degradation. VI. Effect of the primary sequence on the pathways of degradation of aspartyl residues in model hexapeptides, *Pharm. Res. 11*, 751−758.
22. Wright, H. T. (1991) Sequence and structure determinants of the nonenzymatic deamidation of asparagine and glutamine residues in proteins, *Protein Eng. 4*, 283−294.
23. Capasso, S., and Salvadori, S. (1999) Effect of the three-dimensional structure on the deamidation reaction of ribonuclease A, *J. Pept. Res. 54*, 377−382.

24. Bischoff, R., Lepage, P., Jaquinod, M., Cauet, G., Acker-Klein, M., Clesse, D., Laporte, M., Bayol, A., Van, Dorsselaer, A., and Roitsch, C. (1993) Sequence-specific deamidation: isolation and biochemical characterization of succinimide intermediates of recombinant hirudin, *Biochemistry 32*, 725−734.
25. Xie, M., Shahrokh, Z., Kadkhodayan, M., Henzel, W. J., Powell, M. F., Borchardt, R. T., and Schowen, R. L. (2003) Asparagine deamidation in recombinant human lymphotoxin: hindrance by three-dimensional structures, *J. Pharm. Sci. 92*, 869−880.
26. Stevenson, C. L., Friedman, A. R., Kubiak, T. M., Donlan, M. E., and Borchardt, R. T. (1993) Effect of secondary structure on the rate of deamidation of several growth hormone releasing factor analogs, *Int. J. Pept. Protein Res. 42*, 497−503.
27. Otwinowski, Z., and Minor, W. (1997) Processing of x-ray diffraction data collected in oscillation mode, *Methods Enzymol 276*, 307−326.
28. Anonymous. (1994) The CCP4 suite: programs for protein crystallography, *Acta Crystallogr. D Biol. Crystallogr. 50*, 760−763.
29. McCoy, A. J., Grosse-Kunstleve, R. W., Storoni, L. C., and Read, R. J. (2005) Likelihood-enhanced fast translation functions, *Acta Crystallogr. D Biol. Crystallogr. D61*, 458−464.
30. McRee, D. E. (1999) XtalView/Xfit-A Versatile Program for Manipulating Atomic Coordinates and Electron Density, *J. Struct. Biol. 125*, 156−165.
31. Lee, B., and Richards, F. M. (1971) The interpretation of protein structures: estimation of static accessibility, *J. Mol. Biol. 55*, 379−400.
32. Aswad, D. W. (1995) *Deamidation and Isoaspartate Formation in Peptides and Proteins*, CRC Press, Ann Arbor.
33. Kossiakoff, A. A. (1988) Tertiary structure is a principal determinant to protein deamidation, *Science 240*, 191−194.
34. Tetin, S. Y., Prendergast, F. G., and Venyaminov, S. Y. (2003) Accuracy of protein secondary structure determination from circular dichroism spectra based on immunoglobulin examples, *Anal. Biochem. 321*, 183−187.
35. Powell, M. F. (1996) A compendium and hydropathy/flexibility analysis of common reactive sites in proteins: reactivity at Asn, Asp, Gln, and Met motifs in neutral pH solution, *Pharm. Biotechnol. 9*, 1−140.
36. Brennan, T. V., and Clarke, S. (1993) Spontaneous degradation of polypeptides at aspartyl and asparaginyl residues: Effects of the solvent dielectric, *Protein Sci. 2*, 331−338.

BI061500T